

Model Study of Three-Body Forces in the Three-Body Bound State

H. Liu, Ch. Elster

*Institute of Nuclear and Particle Physics, and Department of Physics,
Ohio University, Athens, OH 45701*

W. Glöckle

*Institute for Theoretical Physics II, Ruhr-University Bochum, D-44780 Bochum, Germany.
(December 22, 2018)*

Abstract

The Faddeev equations for the three-body bound state with two- and three-body forces are solved directly as three-dimensional integral equation. The numerical feasibility and stability of the algorithm, which does not employ partial wave decomposition is demonstrated. The three-body binding energy and the full wave function are calculated with Malfliet-Tjon-type two-body potentials and scalar Fujita-Miyazawa type three-body forces. The influence of the strength and range of the three-body force on the wave function, single particle momentum distributions and the two-body correlation functions are studied in detail. The extreme case of pure three-body forces is investigated as well.

PACS number(s): 21.45+v

Typeset using REVTeX

I. INTRODUCTION

Three-body Faddeev equations for the bound state using local forces directly without finite rank expansion have been solved since the pioneering work by Malfliet and Tjon [1] and Osborn [2]. After this, a huge body of work by different groups followed, and calculations using the Faddeev equations were either performed in momentum space, see e.g. [3–5,7], in configuration space [6,8,9], or in a hybrid fashion using both spaces [10]. However, the technique was always based on an angular momentum decomposition, which including spin and isospin degrees of freedom lead to quite a large set of states. For instance allowing NN forces to act in all states of total angular momenta j up to $j=6$, which is necessary to control the ^3H binding energy within 2 keV require 102 angular momentum and isospin combinations (in the literature often called channels). In view of this very large number of interfering terms and having in mind that computer resources are still increasing steadily, it appears natural to give up such an expansion and work directly with momentum vectors or position vectors in configuration space as it is common in Greens Function Monte Carlo methods [11]. We started an approach based on momentum vectors as variables for the three-boson bound state [12], which then could be extended to the three-boson continuum in a straightforward fashion [13]. In configuration space Faddeev equations have been solved applying vector variables for pure Coulomb bound-state problems, namely the $e^-e^-e^+$ and the $pp\mu^-$ systems [14]. Including spin and isospin degrees of freedom together with realistic nucleon-nucleon (NN) forces, a scheme based on momentum vectors has been applied to NN scattering leading to integral equations in two variables [15], which can easily be solved on present day computers.

Angular momentum decompositions even for three bosons require quite a tedious algebra and care in a computational implementation [16] due to often nontrivial cancellations between partial wave terms. This is especially true if one includes three-body forces [17,18]. In contrast, the formulation in terms of momentum vectors of the one Faddeev equation for identical particles is very straightforward and transparent. In this paper we extend the approach from Ref. [12] and include three-body forces for an investigation of the three-body bound state. Because of the ease in solving the Faddeev equation including three-body forces in this fashion, we allow ourselves to explore various combinations of two- and three-body forces of different nature: purely attractive ones, ones with attraction and repulsion and even cases with three-body forces alone. In the latter case we investigate whether wave function properties change qualitatively in comparison to a scenario dominated by two-body forces.

The paper is organized as follows. In Section II the Faddeev equation including two- and three-body forces is formulated in terms of momentum vectors, and its solution, especially the intermediate integrations are layed out in detail. Section III displays our choice of forces and provides the necessary numerical insight for achieving an accurate solution. Wave function properties are displayed in Section IV and different mechanisms for the binding of three-body systems are investigated in Section V. Finally we summarize in Section VI and end with an outlook.

II. THREE-BODY BOUND STATE EQUATION WITH THREE-BODY FORCE

The bound state of three identical particles which interact via pairwise forces $V^i = V_{jk}$ ($i, j, k = 1, 2, 3$ and cyclic permutations thereof) and a genuine three-body force V_{123} is given by the Schrödinger equation which reads in integral form

$$|\Psi\rangle = G_0 \left(\sum_{i=1}^3 V^i + V_{123} \right) |\Psi\rangle. \quad (2.1)$$

Here the free propagator is given by $G_0 = (E - H_0)^{-1}$, where H_0 stands for the free Hamiltonian and E for the binding energy of the three-body system. If the three-body force (3BF) V_{123} is of Fujita-Miyazawa type [19], i.e. consists of two consecutive meson exchanges with a non-nucleonic intermediate state, then it can be decomposed into three different pieces as

$$V_{123} = \sum_{i=1}^3 V_4^{(i)}, \quad (2.2)$$

such that $V_4^{(i)}$ is symmetric under the exchange of particles j and k ($j \neq i \neq k$). The decomposition suggested in Eq. (2.2) is natural for e.g. realistic $\pi\pi$ 3N forces, which are considered at present in all available 3N forces. Introducing Faddeev components $|\Psi\rangle = \sum_{i=1}^3 |\psi_i\rangle$ with

$$|\psi_i\rangle = G_0 (V_i + V_4^{(i)}) |\Psi\rangle \quad (2.3)$$

leads to three coupled integral equations

$$\begin{aligned} |\psi_i\rangle &= G_0 t_i \sum_{j \neq i} |\psi_j\rangle + (1 + G_0 t_i) G_0 V_4^{(i)} \sum_j |\psi_j\rangle \\ &= G_0 \{ t_i \sum_{j \neq i} |\psi_j\rangle + (1 + t_i G_0) V_4^{(i)} \sum_j |\psi_j\rangle \}. \end{aligned} \quad (2.4)$$

The operator t_i describes the two-body t -matrix in the subsystem jk . If we consider identical particles (here bosons, since we are omitting spin), the three-nucleon wave function $|\Psi\rangle$ has to be totally symmetric. As a consequence, the Faddeev components $|\psi_i\rangle$ are identical in their functional form, only the particles are permuted. Thus it is sufficient to consider only one component, e.g.

$$|\psi_1\rangle = G_0 t_1 P |\psi_1\rangle + (1 + G_0 t) V_4^{(1)} (1 + P) |\psi_1\rangle \quad (2.5)$$

In the following the index (1) will be dropped. The permutation operator P is given as $P = P_{12}P_{23} + P_{13}P_{23}$ and the total wave function reads

$$|\Psi\rangle = (1 + P) |\psi\rangle. \quad (2.6)$$

In order to solve Eq. (2.5) standard Jacobi momenta are used,

$$\begin{aligned} \mathbf{p}_i &= \frac{1}{2} (\mathbf{k}_j - \mathbf{k}_k) \\ \mathbf{q}_i &= \frac{2}{3} \left(\mathbf{k}_i - \frac{1}{2} (\mathbf{k}_j + \mathbf{k}_k) \right), \end{aligned} \quad (2.7)$$

where $ijk = 123$ and cyclic permutations thereof. For later clarification we label the coordinates with $ijk = 123$ as system of ‘type (1)’, the ones with $ijk = 231$ as ‘type (2)’ and the ones with $ijk = 312$ as ‘type (3)’. With the Jacobi momenta from Eq. (2.7) and omitting the arbitrarily chosen index 1, Eq. (2.5) reads

$$\langle \mathbf{pq} | \psi \rangle = \frac{1}{E - \frac{\mathbf{p}^2}{m} - \frac{3q^2}{4m}} \langle \mathbf{pq} | tP + V_4(1 + P) + tG_0V_4(1 + P) | \psi \rangle. \quad (2.8)$$

Introducing the symmetrized two-nucleon t -matrix

$$t_s(\mathbf{p}, \mathbf{q}; E) = t(\mathbf{p}, \mathbf{q}; E) + t(-\mathbf{p}, \mathbf{q}; E) \quad (2.9)$$

and explicitly working out the permutation operator P in the first term of Eq. (2.8) leads to

$$\begin{aligned} \langle \mathbf{pq} | \psi \rangle = & \frac{1}{E - \frac{\mathbf{p}^2}{m} - \frac{3q^2}{4m}} \left[\int d^3 q' t_s \left(\mathbf{p}, \frac{1}{2}\mathbf{q} + \mathbf{q}'; E - \frac{3}{4m}q^2 \right) \langle \mathbf{q} + \frac{1}{2}\mathbf{q}', \mathbf{q}' | \psi \rangle \right. \\ & \left. + \langle \mathbf{pq} | V_4(1 + P) | \psi \rangle + \frac{1}{2} \int d^3 \tilde{p} \frac{t_s \left(\mathbf{p}, \tilde{\mathbf{p}}; E - \frac{3}{4m}q^2 \right)}{E - \frac{\tilde{\mathbf{p}}^2}{m} - \frac{3}{4m}q^2} \langle \tilde{\mathbf{pq}} | V_4(1 + P) | \psi \rangle \right] \end{aligned} \quad (2.10)$$

A 3BF of Fujita-Miyazawa type with scalar meson exchanges and a constant meson-nucleon amplitude can be written in the form of Eq. (2.2) with

$$V_4 \equiv V_4^{(1)} \propto \frac{F(Q^2)}{Q^2 + m_s^2} \frac{F(Q'^2)}{Q'^2 + m_s^2} \quad (2.11)$$

and a cutoff function

$$F(Q^2) = \left(\frac{\Lambda^2 - m_s^2}{\Lambda^2 + Q^2} \right)^2. \quad (2.12)$$

The momentum transfer \mathbf{Q} (\mathbf{Q}') is given by

$$\begin{aligned} \mathbf{Q} &= \mathbf{k}_3 - \mathbf{k}'_3 = \mathbf{p} - \mathbf{p}' - \frac{1}{2}(\mathbf{q} - \mathbf{q}') \\ \mathbf{Q}' &= \mathbf{k}'_2 - \mathbf{k}_2 = \mathbf{p} - \mathbf{p}' + \frac{1}{2}(\mathbf{q} - \mathbf{q}'), \end{aligned} \quad (2.13)$$

as indicated in Fig. 1.

For the evaluation of Eq. (2.10) matrix elements of the form $\langle \mathbf{pq} | V_4(1 + P) | \psi \rangle$ need to be calculated. From Fig. 1 we see that V_4 can be considered as a sequence of meson exchanges in the subsystem (12), called for convenience subsystem 3, and subsystem (31), called 2. Inserting a complete set of states of the type 3 between V_4 and $(1 + P) | \psi \rangle$ and another complete set of states of type 2 between the two meson exchanges (see Eq. (2.11)), leads after a straightforward evaluation to

$$\begin{aligned}
\langle \mathbf{p} \mathbf{q} | V_4(1 + P) | \psi \rangle &= \int d^3 q' \frac{F((- \mathbf{p} - \frac{1}{2} \mathbf{q} - \mathbf{q}')^2)}{(- \mathbf{p} - \frac{1}{2} \mathbf{q} - \mathbf{q}')^2 + m_s^2} \\
&\times \int d^3 p' \frac{F((- \mathbf{p} + \frac{1}{2} \mathbf{q} - \frac{1}{2} \mathbf{q}' - \mathbf{p}')^2)}{(- \mathbf{p} + \frac{1}{2} \mathbf{q} - \frac{1}{2} \mathbf{q}' - \mathbf{p}')^2 + m_s^2} \langle \mathbf{p}' \mathbf{q}' | (1 + P) | \psi \rangle
\end{aligned} \tag{2.14}$$

The propagators in Eq. (2.14) contain linear combinations of three or four momentum vectors and thus the two integrations would involve magnitudes of vectors and angles between them. Realizing that both meson-exchange propagators in the 3BF term only depend on the momentum transfer in a two-body subsystem, one can rewrite Eq. (2.14) as

$$\begin{aligned}
\langle \mathbf{p} \mathbf{q} | V_4(1 + P) | \psi \rangle &= \int d^3 p' d^3 q' \langle \mathbf{p} \mathbf{q} | \mathbf{p}' \mathbf{q}' \rangle_2 \\
&\times \int d^3 p'' \frac{F((\mathbf{p}' - \mathbf{p}'')^2)}{(\mathbf{p}' - \mathbf{p}'')^2 + m_s^2} \\
&\times \int d^3 p''' d^3 q''' {}_2 \langle \mathbf{p}'' \mathbf{q}' | \mathbf{p}''' \mathbf{q}''' \rangle_3 \\
&\times \int d^3 p'''' \frac{F((\mathbf{p}''' - \mathbf{p}''''')^2)}{(\mathbf{p}''' - \mathbf{p}''''')^2 + m_s^2} {}_3 \langle \mathbf{p}'''' \mathbf{q}''' | \Psi \rangle.
\end{aligned} \tag{2.15}$$

Here the subscripts 1, 2, 3 of the bra and ket vectors stand for the different types of coordinate systems described by Eq. (2.7). Though the integrations of Eq. (2.15) look more complicated, the meson-propagators show a very simple form. In fact, the integrations over \mathbf{p}'' and \mathbf{p}''' have an identical functional form. Defining

$$F_3(\mathbf{p}''', \mathbf{q}''') = \int d^3 p'''' \frac{F((\mathbf{p}''' - \mathbf{p}''''')^2)}{(\mathbf{p}''' - \mathbf{p}''''')^2 + m_s^2} {}_3 \langle \mathbf{p}'''' \mathbf{q}''' | \Psi \rangle, \tag{2.16}$$

the integration of the meson exchange between particles 2 and 1 in Eq. (2.16) is carried out completely in the coordinate system of type 3. Once $F_3(\mathbf{p}''', \mathbf{q}''')$ is obtained, it needs to be expressed in terms of momenta in a coordinate system of type 2 in order to carry out the integration over the remaining meson exchange. This transformation, labeled $F_{32}(\mathbf{p}'', \mathbf{q}')$ is explicitly given as

$$\begin{aligned}
F_{32}(\mathbf{p}'', \mathbf{q}') &= \int d^3 p''' d^3 q''' {}_2 \langle \mathbf{p}'' \mathbf{q}' | \mathbf{p}''' \mathbf{q}''' \rangle_3 F_3(\mathbf{p}''', \mathbf{q}''') \\
&= F_3\left(|-\frac{1}{2}\mathbf{p}'' - \frac{3}{4}\mathbf{q}'|, |\mathbf{p}'' - \frac{1}{2}\mathbf{q}'|, \frac{(-\frac{1}{2}\mathbf{p}'' - \frac{3}{4}\mathbf{q}') \cdot (\mathbf{p}'' - \frac{1}{2}\mathbf{q}')}{|-\frac{1}{2}\mathbf{p}'' - \frac{3}{4}\mathbf{q}'| |\mathbf{p}'' - \frac{1}{2}\mathbf{q}'|}\right).
\end{aligned} \tag{2.17}$$

Here we used that $F_3(\mathbf{p}''', \mathbf{q}''')$ is a scalar function due to the total wave function $\Psi(\mathbf{p}, \mathbf{q})$ being a scalar in the ground state. The integration over the second meson exchange between particle 1 and 3 in the coordinate system of type 2 is now given by

$$F_2(\mathbf{p}', \mathbf{q}') = \int d^3 p'' \frac{F((\mathbf{p}' - \mathbf{p}'')^2)}{(\mathbf{p}' - \mathbf{p}'')^2 + m_s^2} F_{32}(\mathbf{p}'', \mathbf{q}'). \tag{2.18}$$

The matrix element $\langle \mathbf{p} \mathbf{q} | V_4(1 + P) | \psi \rangle$ is finally obtained by integrating $F_2(\mathbf{p}', \mathbf{q}')$ over \mathbf{p}' and \mathbf{q}' , i.e. carrying out the final coordinate transformation from the system of type 2 back to the one of type 1,

$$\begin{aligned}
\langle \mathbf{p} \mathbf{q} | V_4(1 + P) | \psi \rangle &= \int d^3 p' d^3 q' \langle \mathbf{p} \mathbf{q} | \mathbf{p}' \mathbf{q}' \rangle {}_2 F_2(\mathbf{p}', \mathbf{q}') \\
&= F_2\left(|-\frac{1}{2}\mathbf{p} + \frac{3}{4}\mathbf{q}|, |-\mathbf{p} - \frac{1}{2}\mathbf{q}|, \frac{(-\frac{1}{2}\mathbf{p} + \frac{3}{4}\mathbf{q}) \cdot (-\mathbf{p} - \frac{1}{2}\mathbf{q})}{|-\frac{1}{2}\mathbf{p} + \frac{3}{4}\mathbf{q}| |-\mathbf{p} - \frac{1}{2}\mathbf{q}|}\right).
\end{aligned} \tag{2.19}$$

Thus, the integration of Eq. (2.15), explicitly given in separate steps from Eq. (2.16) to Eq. (2.19) contains only integrations over one vector variable at a time. It should be pointed out that Eqs. (2.17) and Eq. (2.19) are only three dimensional interpolations. Clearly, the in Eq. (2.15) suggested method is the preferred one for practical calculations.

The Faddeev amplitude $\psi(\mathbf{p}, \mathbf{q})$ is given as function of vector Jacobi momenta and obtained as solution of a three dimensional integral equation, Eq. (2.10). For the ground state $\psi(\mathbf{p}, \mathbf{q})$ is also a scalar and thus only depends on the magnitudes of \mathbf{p} and \mathbf{q} and the angle between the two vectors. In order to solve the Eq. (2.10) directly without introducing partial wave projection, we have to define a coordinate system. We choose the vector \mathbf{q} parallel to the z -axis and express the remaining vectors with respect to \mathbf{q} . For the first term in Eq. (2.10) the relevant vectors are \mathbf{p} and \mathbf{q}' . Thus one has aside from the magnitudes the following angle relations

$$\begin{aligned}
x &= \hat{\mathbf{p}} \cdot \hat{\mathbf{q}} = \cos \theta \\
x' &= \hat{\mathbf{q}}' \cdot \hat{\mathbf{q}} = \cos \theta' \\
y &= \hat{\mathbf{p}} \cdot \hat{\mathbf{q}}' = \cos \gamma
\end{aligned} \tag{2.20}$$

where

$$\cos \gamma = \cos \theta \cos \theta' + \sin \theta \sin \theta' \cos(\phi - \phi') = xx' + \sqrt{1 - x^2} \sqrt{1 - x'^2} \cos \phi' \tag{2.21}$$

Since the ϕ' integration is over the full 2π interval we have a freedom of choice for the azimuthal angle angle and set $\phi = 0$. With these choice of variables Eq. (2.10) with only the first term, i.e. two-body forces alone, was solved successfully in Ref [12]. For the evaluation of the second term in Eq. (2.10),

$$\langle \mathbf{p} \mathbf{q} | V_4(1 + P) | \psi \rangle = \langle \mathbf{p} \mathbf{q} | V_4 | \Psi \rangle, \tag{2.22}$$

we start with calculating first $F_3(\mathbf{p}''', \mathbf{q}''')$, Eq. (2.16), and realize, that for this integration we can choose \mathbf{q}''' parallel to the z -axis. With this choice we have as variables the magnitudes of $\mathbf{p}''', \mathbf{p}''''$ and \mathbf{q}''' and the angles between them

$$\begin{aligned}
x''' &= \hat{\mathbf{p}}''' \cdot \hat{\mathbf{q}}''' \\
x'''' &= \hat{\mathbf{p}}'''' \cdot \hat{\mathbf{q}}''' \\
y'''' &= \hat{\mathbf{p}}'''' \cdot \hat{\mathbf{p}}''' = x'''x'''' + \sqrt{1 - x'''^2} \sqrt{1 - x''''^2} \cos \phi'''' ,
\end{aligned} \tag{2.23}$$

where we again can choose the coordinate system such that one of the azimuthal angles can be set to zero. This leads to the explicit expression

$$\begin{aligned}
F_3(p''', q''', x''') &= \\
\int_0^\infty dp'''' p''''^2 \int_{-1}^{+1} dx'''' \int_0^{2\pi} d\phi'''' \frac{\left(\frac{\Lambda^2 - m_\alpha^2}{\Lambda^2 + (p''''^2 + p''''^2 - 2p'''p''''y''''^2)^2}\right)^2}{(p''''^2 + p''''^2 - 2p'''p''''y''''^2)^2 + m_\alpha^2} \Psi(p''', q''', x''').
\end{aligned} \tag{2.24}$$

The evaluation of $F_{32}(\mathbf{p}'', \mathbf{q}')$, Eq. (2.17) is not an integration but rather a three dimensional interpolation and explicitly given by

$$F_{32}(p'', q', x'') = F_3 \left(\frac{1}{2} \sqrt{\frac{9}{4} q'^2 + p''^2 + 3p'' q' x''}, \sqrt{\frac{1}{4} q'^2 + p''^2 - p'' q' x''}, \frac{\frac{3}{8} q'^2 - \frac{1}{2} p''^2 - \frac{1}{2} p'' q' x''}{\left| -\frac{3}{4} \mathbf{q}' - \frac{1}{2} \mathbf{p}'' \right| \left| +\mathbf{p}'' - \frac{1}{2} \mathbf{q}' \right|} \right). \quad (2.25)$$

with

$$\begin{aligned} \left| -\frac{3}{4} \mathbf{q}' - \frac{1}{2} \mathbf{p}'' \right| &= \frac{1}{2} \sqrt{\frac{9}{4} q'^2 + p''^2 + 3p'' q' x''} \\ \left| +\mathbf{p}'' - \frac{1}{2} \mathbf{q}' \right| &= \sqrt{\frac{1}{4} q'^2 + p''^2 - p'' q' x''}. \end{aligned} \quad (2.26)$$

For the interpolation we apply the cubic splines introduced in Ref [18]. The integration over the second meson exchange, i.e. the calculation of $F_2(\mathbf{p}', \mathbf{q}')$ of Eq. (2.18) is functionally the same as Eq. (2.24), since we can choose the variable \mathbf{q}' parallel to the z -axis. Thus we have the same expression as Eq. (2.24) with p', q', x', p'', x'' and ϕ'' instead of p''', q''', x''', p'''' , x'''' and ϕ'''' . Finally, the matrix element $\langle \mathbf{p} \mathbf{q} | V_4 | \Psi \rangle$ is explicitly obtained by a second interpolation as

$$\begin{aligned} \langle \mathbf{p} \mathbf{q} | V_4 | \Psi \rangle &\equiv V_4 \Psi(p, q, x) \\ &= F_2 \left(\frac{1}{2} \sqrt{\frac{9}{4} q^2 + p^2 - 3p q x}, \sqrt{\frac{1}{4} q^2 + p^2 + p q x}, \frac{-\frac{3}{8} q^2 + \frac{1}{2} p^2 - \frac{1}{2} p q x}{\left| +\frac{3}{4} \mathbf{q} - \frac{1}{2} \mathbf{p} \right| \left| -\mathbf{p} - \frac{1}{2} \mathbf{q} \right|} \right) \end{aligned} \quad (2.27)$$

with

$$\begin{aligned} \left| +\frac{3}{4} \mathbf{q} - \frac{1}{2} \mathbf{p} \right| &= \frac{1}{2} \sqrt{\frac{9}{4} q^2 + p^2 - 3p q x} \\ \left| -\mathbf{p} - \frac{1}{2} \mathbf{q} \right| &= \sqrt{\frac{1}{4} q^2 + p^2 + p q x}. \end{aligned} \quad (2.28)$$

The last term of Eq. (2.10) requires an additional integration of the matrix element $\langle \mathbf{p} \mathbf{q} | V_4(1 + P) | \psi \rangle$ and the half shell two body t -matrix. Again, with choosing \mathbf{q} parallel to the z -axis we only have three vectors to consider, $\tilde{\mathbf{p}}$, \mathbf{p} and \mathbf{q} , thus the integration is of a similar type as the one of the first term in Eq. (2.10),

$$\begin{aligned} &\frac{1}{2} \int d^3 \tilde{p} \frac{t_s(\mathbf{p}, \tilde{\mathbf{p}}; E - \frac{3}{4m} q^2)}{E - \frac{\tilde{p}^2}{m} - \frac{3}{4m} q^2} \langle \tilde{\mathbf{p}} \mathbf{q} | V_4(1 + P) | \psi \rangle \\ &= \frac{1}{2} \int_0^\infty d\tilde{p} \tilde{p}^2 \int_1^{+1} d\tilde{x} \int_0^{2\pi} d\tilde{\phi} \frac{t_s(p, \tilde{p}, \tilde{y}_p; E - \frac{3}{4m} q^2)}{E - \frac{\tilde{p}^2}{m} - \frac{3}{4m} q^2} V_4 \Psi(\tilde{p}, q, \tilde{x}) \end{aligned} \quad (2.29)$$

with

$$\begin{aligned}\tilde{x} &= \hat{\tilde{\mathbf{p}}} \cdot \hat{\mathbf{q}} \\ \tilde{y}_p &= \hat{\tilde{\mathbf{p}}} \cdot \hat{\mathbf{p}} = x\tilde{x} + \sqrt{1-x^2}\sqrt{1-\tilde{x}^2} \cos \tilde{\phi}.\end{aligned}\quad (2.30)$$

We obtain the energy eigenvalue E and Faddeev component $\psi(p, q, x)$ of the three-body system by solving Eq. (2.10).

Finally, we want to give the explicit expression for the full wave function from Eq. (2.6), which is

$$\begin{aligned}\Psi(p, q, x) &= \psi(p, q, x) \\ &+ \psi\left(\frac{1}{2}\sqrt{\frac{9}{4}q^2 + p^2 + 3pqx}, \sqrt{\frac{1}{4}q^2 + p^2 - pqx}, \frac{\frac{3}{8}q^2 - \frac{1}{2}p^2 - \frac{1}{2}pqx}{\left|-\frac{3}{4}\mathbf{q} - \frac{1}{2}\mathbf{p}\right| \left|-\frac{1}{2}\mathbf{q} + \mathbf{p}\right|}\right) \\ &+ \psi\left(\frac{1}{2}\sqrt{\frac{9}{4}q^2 + p^2 - 3pqx}, \sqrt{\frac{1}{4}q^2 + p^2 + pqx}, \frac{-\frac{3}{8}q^2 + \frac{1}{2}p^2 - \frac{1}{2}pqx}{\left|+\frac{3}{4}\mathbf{q} - \frac{1}{2}\mathbf{p}\right| \left|-\frac{1}{2}\mathbf{q} - \mathbf{p}\right|}\right).\end{aligned}\quad (2.31)$$

Here the magnitudes of vectors are given by

$$\begin{aligned}\left|+\frac{3}{4}\mathbf{q} \pm \frac{1}{2}\mathbf{p}\right| &= \frac{1}{2}\sqrt{\frac{9}{4}q^2 + p^2 \pm 3pqx}, \\ \left|-\frac{1}{2}\mathbf{q} \pm \mathbf{p}\right| &= \sqrt{\frac{1}{4}q^2 + p^2 \pm pqx}.\end{aligned}\quad (2.32)$$

The wave function is normalized according to

$$\int d^3p d^3q \Psi^2(\mathbf{p}, \mathbf{q}) = 1. \quad (2.33)$$

III. CALCULATION OF THE THREE-BODY BOUND STATE

Our model calculations are based on Yukawa interactions. As two-body force (2BF) we employ a Malfliet-Tjon [1] type potential

$$\begin{aligned}V(\mathbf{q}, \mathbf{q}') &= -\frac{g_A^2}{(2\pi)^3} \frac{1}{(\mathbf{q} - \mathbf{q}')^2 + m_A^2} \left(\frac{\Lambda_A^2 - m_A^2}{(\mathbf{q} - \mathbf{q}')^2 + \Lambda_A^2} \right)^2 \\ &+ \frac{g_R^2}{(2\pi)^3} \frac{1}{(\mathbf{q} - \mathbf{q}')^2 + m_R^2} \left(\frac{\Lambda_R^2 - m_R^2}{(\mathbf{q} - \mathbf{q}')^2 + \Lambda_R^2} \right)^2,\end{aligned}\quad (3.1)$$

which is modified by a cutoff function of dipole type. With this choice, the 2BF and the 3BF have similar functional forms for the scalar meson exchanges. The force in Eq.(3.1) is a superposition of a short-ranged repulsive and long-ranged attractive Yukawa interactions. The coupling constants and exchanged meson masses are characterized by subscripts R and A respectively. The exchanged masses m_A and m_R are those from the original Malfliet-Tjon model, the coupling constants are chosen so that the two-body force gives a binding of the three-body system which is slightly smaller than the experimental value of the triton

binding, which is 8.48 MeV. The cutoff masses Λ have values typical for one-boson-exchange models. The parameters for the 2BF, named MT2-II, are given in Table I.

With this interaction we first solve the Lippmann-Schwinger equation for the fully-off-shell two-body t -matrix directly as function of vector variables as described in Ref. [21]. This t -matrix is then symmetrized to obtain $t_s(p', p, x, E - \frac{3}{4m}q^2)$. The eigenvalue equation, Eq. (2.10), for the three-body bound state is solved iteratively by a Lanczo's type algorithm described in detail in Ref. [4]. Using the 2BF alone, the binding energy of the three-body system is calculated as $E = 7.6986$ MeV.

The simplest 3BF we want to apply in our study has the functional form

$$V_4 = \frac{1}{(2\pi)^6} \frac{a_\alpha}{m_\alpha} g_\alpha^2 \frac{F_\alpha(Q^2)}{Q^2 + m_\alpha^2} \frac{F_\alpha(Q'^2)}{Q'^2 + m_\alpha^2}, \quad (3.2)$$

where

$$F_\alpha(Q^2) = \left(\frac{\Lambda_\alpha^2 - m_\alpha^2}{\Lambda_\alpha^2 + Q^2} \right)^2. \quad (3.3)$$

Choosing a_α to be a negative constant makes this force purely attractive. The parameters of this force, which we name MT3-I in the following, are given in Table II. They are chosen to give a small attractive contribution to the three-body binding energy, which we calculate as $E = 8.8732$ MeV. Though this value is slightly larger than the experimental one for ${}^3\text{H}$, we chose not to readjust it any further for this model study. Our value is close enough to extract qualitative insight, and to act as reference point for our additional studies.

In order to solve the eigenvalue equation, Eq. (2.10), for the Faddeev component $\psi(p, q, x)$, we use Gaussian grid points in p , q , and x . The momentum and angle grids in the integrations of the 3BF in Eqs. (2.24) and (2.29) have the same sizes as the ones for p , q , and x . This is very reasonable, since the integrations over the meson exchange contributions of the 3BF, Eq. (2.24), require grids similar in range to the one used to calculate the two-body t -matrix. The p -grid is defined between 0 and $p_{max} = 60\text{ fm}^{-1}$, whereas for the q -grid a maximum value $q_{max} = 40\text{ fm}^{-1}$ is sufficient. For the angle (x) integration, the preferred number is 42 grid points. Further details concerning the grid choices are given in Ref. [12]. Typical grid sizes are $97 \times 97 \times 42$ to obtain an accuracy in the binding energy of 5 significant figures. The convergence of the three-body binding energy E as function of the number of grid points is shown in Table III, where we see a convergence of the energy eigenvalue and the expectation values within 5 digits.

The three-body wave function is calculated from the Faddeev component using Eq. (2.31). Since this wave function enters the eigenvalue equation, Eq. (2.10), we also need to worry about the quality of the calculation of $\Psi(p, q, x)$. One check of the overall quality of the wave function is a comparison of the expectation value of the total Hamiltonian $\langle H \rangle$ with the calculated value E from the solution of the Faddeev equation. Explicitly, we evaluate

$$\langle H \rangle \equiv \langle \Psi | H | \Psi \rangle = \langle \Psi | H_0 | \Psi \rangle + \langle \Psi | V_{II} | \Psi \rangle + \langle \Psi | V_{123} | \Psi \rangle, \quad (3.4)$$

where V_{II} represents the 2BF $\sum_{i=1}^3 V^i$ and V_{123} the three-body defined in Eq. (2.2). The expectation value of the kinetic energy $\langle H_0 \rangle$ and the two-body potential energy $\langle V_{II} \rangle$ are given as [12]

$$\begin{aligned}
\langle H_0 \rangle &\equiv \langle \Psi | H_0 | \Psi \rangle = 3 \langle \psi | H_0 | \Psi \rangle \\
&= 3 \cdot 8\pi^2 \int_0^\infty p^2 dp \int_0^\infty q^2 dq \left(\frac{p^2}{m} + \frac{3q^2}{4m} \right) \int_{-1}^{+1} dx \psi(p, q, x) \Psi(p, q, x)
\end{aligned} \tag{3.5}$$

and

$$\begin{aligned}
\langle V_{II} \rangle &\equiv \langle \Psi | V_{II} | \Psi \rangle = 3 \langle \Psi | V^1 | \Psi \rangle \\
&= 3 \cdot 8\pi^2 \int_0^\infty p^2 dp \int_0^\infty q^2 dq \int_{-1}^{+1} dx \int_0^\infty p'^2 dp' \int_{-1}^{+1} dx' \\
&\quad \times \Psi(p, q, x) v_1(p, p', x, x') \Psi(p', q, x')
\end{aligned} \tag{3.6}$$

where

$$v_1(p, p', x, x') = \int_0^{2\pi} d\phi V^1(p, p', xx' + \sqrt{1-x^2}\sqrt{1-x'^2} \cos \phi). \tag{3.7}$$

The expectation value of the three-body potential energy, $\langle V_{123} \rangle$, is given by

$$\begin{aligned}
\langle V_{123} \rangle &\equiv \langle \Psi | V_{123} | \Psi \rangle = 3 \langle \Psi | V_4 | \Psi \rangle \\
&= 3 \cdot 8\pi^2 \int_0^\infty p^2 dp \int_0^\infty q^2 dq \int_{-1}^{+1} dx \Psi(p, q, x) V_4 \Psi(p, q, x).
\end{aligned} \tag{3.8}$$

Here the integrations need the evaluation of the matrix element $\langle \mathbf{p} \mathbf{q} | V_4 | \Psi \rangle$ of Eq. (2.7). The expectation values of the kinetic and potential energies are listed in Table III as functions of the size of the $p-q-x$ grid. Table III shows that the expectation values given above converge for 5 significant figures when the grid sizes for p and q exceed 77 points. However, Table III also shows that the expectation value $\langle H \rangle$ does not exactly converge to the calculated value E despite increased grid size. The difference between the two quantities is of the order of 10 keV. This behavior is in contrast to calculations based solely on two-body forces. Calculations with $V_{123} = 0$ are shown in Table IV as function of the size of the $p-q-x$ grid. Here the convergence of $\langle H \rangle$ to the calculated value E as function of the grid size is much better than in the case where an attractive 3BF is included.

It is well known that three nucleon forces based on multi-meson exchanges can have attractive as well as repulsive pieces. Thus we also consider a model of this type given as

$$\begin{aligned}
V_4 &= \frac{1}{(2\pi)^6} \frac{a_\alpha}{m_\alpha} g_\alpha^2 \frac{F_\alpha(Q^2)}{Q^2 + m_\alpha^2} \frac{F_\alpha(Q'^2)}{Q'^2 + m_\alpha^2} \\
&+ \frac{1}{(2\pi)^6} \frac{a_{\alpha\rho}}{\sqrt{m_\alpha m_\rho}} g_\alpha g_\rho \left(\frac{F_\alpha(Q^2)}{Q^2 + m_\alpha^2} \frac{F_\rho(Q'^2)}{Q'^2 + m_\rho^2} + \frac{F_\rho(Q'^2)}{Q'^2 + m_\rho^2} \frac{F_\alpha(Q^2)}{Q^2 + m_\alpha^2} \right).
\end{aligned} \tag{3.9}$$

Here the first term represents an attractive force, characterized by a negative coupling a_α , whereas the second term represent a repulsive force, i.e. $a_{\alpha\rho}$ is positive. Since the masses of the exchange mesons are different, the form of the second, repulsive term guarantees that V_4 is symmetric under a permutation of nucleons 2 and 3. The cutoff functions F_α and F_ρ have the same functional form as given in Eq. (3.3). The parameters of this 3BF, named MT3-II in the following, are given in Table V. They are chosen so that the correction due

to this 3BF to the three-body binding energy calculated with the 2BF MT2-II is small. The binding energy E with this MT3-II 3BF gives $E = 8.6478$ MeV.

The expectation values of the kinetic and potential energies are listed in Table VI as functions of the size of the $p - q - x$ grid. Again, the expectation values converge within five significant figures when the grid sizes for p and q exceed 77 points. However, now the difference of the expectation value for the total Hamiltonian $\langle H \rangle$ deviates from the calculated eigenvalue E only by 5 keV, a number being similar to calculations carried out in a partial wave decomposition and based on realistic forces [22].

IV. EFFECTS OF THE THREE-BODY FORCE ON BOUND STATE PROPERTIES AND EXPECTATION VALUES

A. Momentum Distributions and Expectation Values

The three-body force MT3-I introduced in Eq. (3.2) and Table II is of scalar type and purely attractive. Its strength is mainly determined by the overall coupling a_α and the coupling constant g_α , the range is determined by the mass m_α of the exchange particle. In order to study effects of this 3BF on the bound state wave function, we want to consider the momentum distribution $n(q)$, i.e. the probability of finding a nucleon with momentum q in the nucleus. In our case $n(q)$ is given by

$$n(q) = 2\pi q^2 \int_0^\infty dp p^2 \int_{-1}^{+1} dx \Psi^2(p, q, x). \quad (4.1)$$

The total wave function $\Psi(p, q, x)$ is given by Eq. (2.31). It is interesting to study the change in the momentum distribution as function of the strength a_α and the range given by m_α of the 3BF. The effect of an increased strength a_α of the force MT3-I is shown in Fig. 2, and the corresponding changes in the binding energy in Table VII. The momentum distributions calculated with and without the 3BF (where the coupling strength is given by a_α) are nearly the same. This has been noticed before in the context of realistic NN forces [22]. In addition, the shoulder of the distribution around $2-4$ fm $^{-1}$ is qualitatively similar to the case when using realistic forces. Fig. 2 shows that the increase of the 3BF affects the position of the minimum and the high momentum components. In fact, the curve, representing the calculation in which the strength a_α is multiplied by 6, does not show a clear defined minimum any longer. In this case the expectation value of the 3BF becomes larger than the one of the 2BF, as is shown in Table VII. If the strength of the 3BF is increased further, $n(q)$ loses all its structure.

In Fig. 3. we display the effect of the 3BF MT3-I when its range is increased, i.e. the mass m_α of the exchange meson is successively decreased. Again, the minimum of the momentum distribution is shifted towards higher momenta, when the 3BF becomes longer ranged. But in contrast to Fig. 2, the minimum is preserved in all cases. The corresponding increase in the binding energy is indicated in Table X.

Next we consider the effects of the 3BF MT3-II, which in addition has a repulsive core. The corresponding momentum distributions $n(q)$ are displayed in Fig. 4. Here we study the effect on the momentum distribution $n(q)$ obtained when successively increasing both coupling constants a_α and $a_{\alpha\rho}$ by the same integer multiple. The corresponding changes

in the binding energy are given in Table VIII. As seen before, an increase of the coupling parameters of the 3BF shifts the minima of the distribution to higher values of q . It is interesting to notice that despite the increase in the strength of the 3BF, the momentum distribution keeps its minimum. This can be explained by the fact that the ratio between repulsion and attraction within the 3BF is preserved. If we would have increased only the attraction, the situation would be similar to the one shown in Fig. 2.

When increasing the strength of the 3BF, it is obvious that the binding energy of the three-body system also increases. It is illustrative to compare the influence of the two different types of three-body forces, MT3-I and MT3-II, on the expectation values of the kinetic energy $\langle H_0 \rangle$, the two-body potential energy $\langle V_{II} \rangle$ and the three-body potential energy $\langle V_{123} \rangle$. In Table VII these expectation values are listed for calculations based on the 2BF MT2-II and the purely attractive 3BF MT3-I. As expected, the binding energy E increases as the strength of the 3BF increases. Similarly, the expectation values $\langle H_0 \rangle$ and $\langle V_{123} \rangle$ increase. In contrast, the expectation value for the two-body potential energy $\langle V_{II} \rangle$ decreases considerably, indicating the decreasing importance of the 2BF for the binding of the system. This is quite different for the case in which the 3BF also has a repulsive core. The expectation values based on calculations using the MT3-II 3BF are shown in Table VIII. For the expectation values given in Table VIII both couplings of the 3BF are increased simultaneously, thus the ratio between attraction and repulsion is roughly maintained.

B. Two-Body Correlation Functions

Bound state properties like the momentum distribution are most naturally derived from wave functions given in momentum space. However, it may also prove insightful to consider properties like correlation functions, which are naturally defined in configuration space. The total wave function in configuration space, $\Psi(\mathbf{r}, \mathbf{R})$, can be calculated as

$$\Psi(\mathbf{r}, \mathbf{R}) = \int d^3p \, d^3q \, \Psi(\mathbf{p}, \mathbf{q}) \exp(i\mathbf{p} \cdot \mathbf{r}) \exp(i\mathbf{q} \cdot \mathbf{R}). \quad (4.2)$$

Here $\Psi(\mathbf{p}, \mathbf{q})$ is the total wave function in momentum space as given by Eq. (2.6). The variables \mathbf{r} and \mathbf{R} are conjugate to the Jacobi momenta \mathbf{p}, \mathbf{q} and given as

$$\begin{aligned} \mathbf{r} &= \mathbf{x}_2 - \mathbf{x}_3, \\ \mathbf{R} &= \mathbf{x}_1 - \frac{1}{2}(\mathbf{x}_2 + \mathbf{x}_3). \end{aligned} \quad (4.3)$$

where $\mathbf{x}_1, \mathbf{x}_2$ and \mathbf{x}_3 are the coordinates of three nucleons in configuration space [16].

For the explicit calculation of the double Fourier transformation we first consider the \mathbf{q} -integration

$$\int d^3q \exp(i\mathbf{q} \cdot \mathbf{R}) \Psi(\mathbf{p}, \mathbf{q}). \quad (4.4)$$

We choose the vector \mathbf{p} parallel to the z-axis and define the angles $\hat{\mathbf{q}} \cdot \hat{\mathbf{z}} = x_q$ and $\hat{\mathbf{R}} \cdot \hat{\mathbf{z}} = x_R$. Since the integration is carried out over all space, we can set $\phi_R = 0$, and obtain

$$\begin{aligned} & \int d^3q \exp(i\mathbf{q} \cdot \mathbf{R}) \Psi(\mathbf{p}, \mathbf{q}) \\ &= \int_0^\infty q^2 dq \int_{-1}^{+1} dx_q \int_0^{2\pi} d\phi_q \exp(iqR\hat{\mathbf{R}} \cdot \hat{\mathbf{q}}) \Psi(p, q, x_q), \end{aligned} \quad (4.5)$$

where

$$\hat{\mathbf{R}} \cdot \hat{\mathbf{q}} = x_q x_R + \sqrt{1 - x_q^2} \sqrt{1 - x_R^2} \cos \phi_q. \quad (4.6)$$

Thus, the integration over ϕ_q can be carried out separately

$$\begin{aligned} & \int_0^{2\pi} d\phi_q \exp(iqR\sqrt{1 - x_q^2} \sqrt{1 - x_R^2} \cos \phi_q) \\ &= 2\pi J_0(qR\sqrt{1 - x_q^2} \sqrt{1 - x_R^2} \cos \phi_q). \end{aligned} \quad (4.7)$$

Summarizing the above leads to the intermediate result

$$\begin{aligned} & \int d^3q \exp(i\mathbf{q} \cdot \mathbf{R}) \Psi(\mathbf{p}, \mathbf{q}) \\ &= 2\pi \int_0^\infty q^2 dq \int_{-1}^{+1} dx_q J_0(qR\sqrt{1 - x_q^2} \sqrt{1 - x_R^2} \cos \phi_q) \exp(iqR x_q x_R) \Psi(p, q, x_q) \\ &\equiv 2\pi \Psi_p(p, R, x_R). \end{aligned} \quad (4.8)$$

Next, we consider the integration over \mathbf{p} , where it is convenient to choose the vector \mathbf{r} parallel to the z-axis. Thus, the following angle, $\hat{\mathbf{R}} \cdot \hat{\mathbf{z}} \equiv \hat{\mathbf{R}} \cdot \hat{\mathbf{r}} \equiv x_R$, needs to be considered, and the integration over x_p and ϕ_p can be carried out separately as

$$\int_{-1}^{+1} dx_p \int_0^{2\pi} d\phi_p \exp(iprx_p) = 4\pi \frac{\sin(pr)}{pr} \quad (4.9)$$

Finally, the Fourier transform of $\Psi(p, q, \hat{\mathbf{p}} \cdot \hat{\mathbf{q}})$ can be calculated as

$$\Psi(r, R, x_R) = \frac{8\pi^2}{r} \int_0^\infty dp [\sin(pr)p \Psi_p(p, R, x_R)], \quad (4.10)$$

where

$$\Psi_p(p, R, x_R) = \int_0^\infty q^2 dq \int_{-1}^{+1} dx_q J_0\left(qR\sqrt{1 - x_q^2} \sqrt{1 - x_R^2}\right) \cos(qR x_q x_R) \Psi(p, q, x_q). \quad (4.11)$$

With this the two-body correlation function $c(r)$ is defined as

$$c(r) = 2\pi r^2 \int_0^\infty dR R^2 \int_{-1}^{+1} dx_R \Psi^2(r, R, x_R). \quad (4.12)$$

The correlation function $c(r)$ describes the probability to find two nucleons within a relative distance r . As for the momentum distribution in the previous subsection, we want to study the effect of changes in the 3BF on the correlation functions. First we consider the purely attractive 3BF MT3-I and increase its strength. The change in the correlation function $c(r)$ is shown in Fig. 5. First, we want to comment that the correlation function $c(r)$ with the 3BF with coupling strength a_α is qualitatively similar to calculations based on realistic forces

[23]. When increasing the coupling strength, we see two correlated effects. The increase in the binding energy leads to a faster fall-off of $c(r)$, and as a further consequence of the fixed normalization to a stronger peaking at small distances. That is, with the increase in binding the system shrinks in size. Next we increase the range of the force by decreasing the mass m_α of the exchange meson. The corresponding changes in the $c(r)$ are shown in Fig. 6. In both cases the 3BF becomes stronger and thus the relative distance between two nucleons decreases, i.e. the three-body system shrinks in size. For the three-nucleon force MT3-II, the situation is quite similar, when both couplings are increased simultaneously. The corresponding correlation functions $c(r)$ are given in Fig. 7.

Since our three-body system consists of three identical nucleons acted on by scalar forces, the three nucleons form a ground state where the most probable positions of the nucleons have the shape of an equilateral triangle. The expectation values of the Jacobi coordinates r and R can be calculated as

$$\begin{aligned}\langle r \rangle &= \int_0^\infty R^2 dR \int_0^\infty r^2 dr \int_{-1}^{+1} dx_R r \Psi^2(r, R, x_R), \\ \langle R \rangle &= \int_0^\infty R^2 dR \int_0^\infty r^2 dr \int_{-1}^{+1} dx_R R \Psi^2(r, R, x_R).\end{aligned}\quad (4.13)$$

Here the values $\langle r \rangle$ and $\langle R \rangle$ are the length and height of the equilateral triangle. The geometrical relation between the length and height of an equilateral triangle is given by

$$\langle r \rangle : \langle R \rangle = \sqrt{3} : 2. \quad (4.14)$$

We also define a deviation δ by

$$\delta = \frac{\langle r \rangle / \langle R \rangle - \sqrt{3}/2}{\sqrt{3}/2} \times 100. \quad (4.15)$$

to account for deviations from an ideal geometric triangle. The binding energy E and the expectation values $\langle r \rangle$ and $\langle R \rangle$ are listed together with the deviation δ in Table IX. The calculations are carried out with the purely attractive 3BF MT3-I, where the coupling a_α is increased by factors 2, 3, and 4. As expected, E increases when a_α is increased. At the same time the expectation values $\langle r \rangle$ and $\langle R \rangle$ become smaller, indicating that the spatial extension of the ground state of the three-body system decreases. The deviation parameter δ remains constant, indicating that the shape of an equilateral triangle is preserved. The decreasing values for $\langle r \rangle$ given in Table IX are consistent with the shifting of the peak of $c(r)$ towards smaller values of r for increasing binding energy. A very similar situation occurs when the range of the MT3-I force is increased by a decrease in the mass m_α of the exchanged meson. The corresponding expectation values for $\langle r \rangle$ and $\langle R \rangle$ are given in Table X. Again the stronger 3BF makes the ground state of the three-body system shrink in size while preserving its spatial shape.

V. DIFFERENT MECHANISMS FOR BINDING THE THREE-BODY SYSTEM

In the previous Section we discussed the behavior of momentum distributions, expectation values and correlation function when successively increasing the influence of the 3BF. In

addition it will be interesting to consider different ‘limiting cases’, in which the three-body bound state is formed either by two-body forces or three-body forces. When considering the nuclear force, we are used to the notion that the 2BF is the dominant one, and three-body forces are considered to give a correction to the binding. Here we want to consider two different types of 2BFs. The first is the MT2-II force, whose parameters are listed in Table I, and which consists of a short ranged, repulsive core and a long range attractive part. The three-body binding energy E given by this MT2-II force is listed in Table XIV together with the expectation values for the kinetic energy $\langle H_0 \rangle$ and the potential energy $\langle V_{II} \rangle$. A second type of scalar potential supporting a three-body bound state is a purely attractive 2BF. We adjusted the parameters of this force, named MT2-I, so that the binding energy E is roughly the same as for the MT2-II force. The resulting parameters are given in Table XI. The corresponding expectation values for the kinetic and potential energies are given in Table XIV. From this table it is obvious, that the latter expectation values are much larger for an attractive potential compared to the potential with a repulsive core.

It is now interesting to consider two cases, in which the three-body system is only bound by a three-body force. Similarly to the two-body forces, we construct two different three-body potentials, which give roughly the same binding energy as the two-body potentials. The first three-body potential, named MMT3-I, is purely attractive. Its parameters are given in Table XII. The second three-body potential, named MMT3-II, consists of a long ranged attraction and a short ranged repulsion. Its parameters are given in Table XIII. The corresponding binding energies E are listed in Table XIV together with the expectation values for the kinetic and potential energies. In addition, the expectation values for the Jacobi coordinates $\langle r \rangle$ and $\langle R \rangle$ are given to indicate the size of the ground state. In the choice of parameters we kept the masses and form factors parameters the same, and adjusted only the strengths to achieve roughly the same binding in all cases. It is interesting to notice that the 3BF MMT3-I leads to much larger expectation values for the kinetic and potential energies than in the case if this 3BF is combined with a 2BF (see the values for $6a_\alpha$ in Table VII). At the same time, the binding energy is drastically reduced, whereas the expectation value of $\langle r \rangle$ peaks at a smaller value, as seen when comparing the short dashed line in Fig. 9 with the dotted line in Fig. 5. In the case of MMT3-II the size is larger than for MMT3-I, but still smaller than the sizes of the systems bound by two-body forces only. The expectation values compared to MMT3-I are reduced by roughly a factor of two.

The momentum distributions $n(q)$ for the four different cases are shown in Fig. 8. For both attractive force models $n(q)$ has no structure, the attractive 3BF produces much higher momentum components. Both models with a repulsive core exhibit a characteristic minimum. However, in the case of the 3BF, this minimum is pushed out to almost double the distance compared to the distribution calculated from the 2BF. The two-body correlation functions $c(r)$ are displayed in Fig. 9. Comparing the correlation functions based on the three-body forces to the ones based on two-body forces, it is very clear, that both 3BFs give a smaller ground state in configuration space and lead to higher momentum components in momentum space.

The full wave functions for the different cases are shown in Fig. 10 for the MT2-I model, in Fig. 11 for the MT2-II model, in Fig. 12 for the MMT3-I model and in Fig. 13 for the MMT3-II model. First, it should be noted that only forces with a repulsive core produce a nodal structure in the wave function. Next, we want to remark that in the case of the

MT2-II model (Fig. 11) the node along the $q = 0$ line corresponds roughly to the node in the two-body potential $V(p, 0)$. For the 3BF MMT3-II there is no such simple connection due to its more complicated structure. However, when considering the expression for the matrix element $\langle \mathbf{p}\mathbf{q}|V_4(1+P)|\psi\rangle$ given in Eq. (2.14), omitting the integrations over \mathbf{q}' and \mathbf{p}' and setting their values to zero, one is left with an expression where the matrix element is only a function of \mathbf{p} and \mathbf{q} and the angle between the two vectors. This matrix element has a strong angle dependence, which is consistent with the observation, that in calculations based on a partial wave expansion, one needs considerably many angular momentum states to achieve a converged result. However, after the integration over this angle, the matrix element, now a function of the magnitudes of the vectors only, displays already a nodal structure similar to the full wave function shown in Fig. 13.

The different models based on two- and three-body forces introduced above show a very distinct character as far as momentum distributions and correlation functions are concerned, although they share roughly the same binding energy. Thus, the binding mechanism could be easily distinguished, e.g. by extracting information about the momentum distribution. Now it is logical to ask, if it is possible to e.g. represent the momentum distribution $n(q)$ of the model MT2-I with two-body forces by a momentum distribution derived from a model based on three-body forces alone. Of course, the binding energy should also be identical. When adjusting the parameters of the MMT3-I force suitably, we actually can achieve this. We consider two different cases. In the first, named (A), the momentum distribution $n(q)$ is overall close to the one of the MT2-I 2BF for a momentum range up to about 6 fm^{-1} . For the second case, named (B), we put special emphasis on a good description of the low momentum range (up to $q \approx 2.5 \text{ fm}^{-1}$). The momentum distributions are shown in Fig. 14. The corresponding correlation functions are shown in Fig. 15. One can read off that for the case (B), the radius of the system is exactly the same as calculated by the 2BF MT2-I. For case (A) the system becomes a tiny bit smaller. In contrast to the previous studies, we had to change the mass of the exchanged meson in order to modify the shape of the momentum distribution. The relevant parameters for case (A) are $m_\alpha = 100 \text{ MeV}$, $\Lambda_\alpha = 700 \text{ MeV}$, and $a_\alpha = -2.82735$, for case (B) those parameters are $m_\alpha = 60 \text{ MeV}$, $\Lambda_\alpha = 660 \text{ MeV}$, and $a_\alpha = -1.90015$. The expectation values for the kinetic and potential energies are in case of (A), $\langle H_0 \rangle = 93.916 \text{ MeV}$ and $\langle V \rangle = -101.497 \text{ MeV}$, and in case of (B), $\langle H_0 \rangle = 67.306 \text{ MeV}$ and $\langle V \rangle = -74.895 \text{ MeV}$. Especially for the latter case, these expectation values are very close to the ones for the 2BF model MT2-I given in Table XIV. From this study we conclude that from wave function properties and binding energies alone one cannot deduce whether the system is bound by two- or three-body forces.

VI. SUMMARY AND OUTLOOK

We derived and calculated the Faddeev equation for three identical bosons interacting by two- and three-body forces. The equation is formulated in momentum space directly in terms of momentum vectors, i.e. without angular momentum decomposition. It is demonstrated that this equation can be solved by integrating over magnitudes of momenta and various angles. In doing so we encounter interpolations which are carried out by cubic Hermitian splines [18]. The Faddeev equation is solved by iteration using a Lanczo's type method [4,24]. An accuracy of 5 digits in the energy eigenvalue can easily be achieved. In comparison to an

angular momentum decomposition which is commonly used [16], this direct approach has great advantages. It avoids the very involved angular momentum algebra occurring for the permutations and especially for the three-body forces [17,18].

Because of the ease of solving the bound state equation we investigated several force scenarios, some of which are purely of academic curiosity. All two- and three-body forces are of meson exchange type, either purely attractive or attractive and repulsive. The mesons responsible for the attraction have masses around 300 MeV, the ones for the repulsion around 600 MeV. These forces, serving as a reference, are chosen with a view towards nuclear physics. Thus the reference two-body forces lead to a three-body binding energy somewhat smaller than 8.48 MeV (the experimental ^3H binding energy), and the reference three-body forces add about 1 MeV additional binding energy.

For these type of forces we evaluated the single nucleon momentum distributions and the two-body correlation functions. These quantities turned out to be qualitatively very similar to what is achieved with realistic spin dependent forces [22,23]. Then we changed the strength parameters and masses of the exchange mesons in the three-body forces to study the changes in the binding energies and in the wave function properties mentioned above. In case that the relative weight of a purely attractive 3BF increases with respect to the 2BF, which has attractive and repulsive parts, the minimum in the momentum distribution and the adjacent shoulder at higher momenta diminish and finally disappear altogether. If, on the other hand, the 3BF has also repulsive parts in addition to the attractive ones, the typical structures of a minimum and a shoulder remain. However, both structures are shifted towards higher momenta.

The two-body correlation functions show the expected behavior, namely that with increasing binding energy the position of the peak of highest probability as well as its widths move to smaller values.

We also evaluated the expectation values $\langle r \rangle$ for a pair distance and $\langle R \rangle$ for the distance of a third particle to the c.m. of the corresponding pair. In case of an equilateral triangle the ratio of these two quantities is $\sqrt{3}/2$. Since we have three identical bosons the position of the three particles in the ground state should be with highest probability at the corners of an equilateral triangle. Indeed the corresponding ratio for the expectation values $\langle r \rangle$ and $\langle R \rangle$ turned out to be $\sqrt{3}/2$ with an numerical error of about 1-2%.

In addition, we investigated the more academic case that only a three-body force binds the system. We chose a purely attractive one and one with attraction and repulsion. If one keeps the meson masses the same, one can trivially achieve a three-body binding energy around 8.5 MeV by an appropriate choice of strength parameters. However, in this case the systems shrinks dramatically in size, and the momentum distributions also change quite drastically in relation to the standard combination of two- and three-body forces.

Finally we investigated whether three-body forces can be found, which lead to about the same binding energy, momentum distribution and correlation function as the ones obtained from a given two-body force. This could indeed be achieved. Thus, from the point of view of wave function properties one can not distinguish whether the underlying forces are of two-body or three-body nature.

Including spin (and isospin) degrees of freedom is an additional task for the future, which will increase the space of states and will lead to coupled equations, but only a strictly finite number of equations. The form in which they will appear will depend on the way the

spin degrees of freedom will be incorporated. One possibility will be the extension of the helicity formalism chosen for the NN system in a three-dimensional notation [15] to three nucleons. The other possible extension of the here presented formulation is the incorporation of relativity in the instant form of dynamics [25]. The momentum space formulation seems ideal for that. First steps have been already undertaken [26]. Since relativity will be of importance at higher energies our treatment with momentum vectors and avoiding angular momentum decomposition will be rewarding in that respect.

ACKNOWLEDGMENTS

This work was performed in part under the auspices of the U. S. Department of Energy under contract No. DE-FG02-93ER40756 with Ohio University. The computational support of the Ohio Supercomputer Center (OSC) for the use of their facilities under Grant No. PHS206, the Neumann Institute for Computing (NIC) under project JIKP01 and the National Energy Research Supercomputer Center (NERSC) is acknowledged. The authors want to thank A. Nogga for helpful and stimulating discussions.

REFERENCES

- [1] R.A. Malfliet, A.J. Tjon, Nucl. Phys. A, **127**, 161 (1969).
- [2] T.A. Osborn, 'Faddeevs Equations for local potentials, SLAC Report No. 17 (1967).
- [3] A. Picklesimer, R.A. Rice, and R. Brandenburg, Phys. Rev C**45**, 2045 (1992), *ibid*, 547 (1992), Phys. Rev. C**44**, 1359 (1991).
- [4] A. Stadler, W. Glöckle, P.U. Sauer, Phys. Rev. C**44**, 2319 (1991);
- [5] A. Stadler and P.U. Sauer, Phys. Rev. C**46**, 64 (1992).
- [6] A. Laverne, C. Gignoux, Nucl. Phys. **A203**, 597 (1973).
- [7] A. Nogga, D. Hüber, H. Kamada, W. Glöckle, Phys. Lett. B **409**, 19 (1997).
- [8] J.L. Friar, B.F. Gibson, and G.L. Payne, Z. Phys. A **301**, 309 (1981), C.R. Chen, G.L. Payne, J.L. Friar, B.F. Gibson, Phys. Rev. C**31**, 2266 (1985).
- [9] N.W. Schellingerhout, L.P. Kok, and G.D. Bosveld, Phys. Rev. A**40**, 5568 (1989); N.W. Schellingerhout, J.J. Schut, and L.P. Kok, Phys. Rev. C**46**, 1192 (1992).
- [10] Y. Wu, S. Ishikawa, T. Sasakawa, Few-Body Systems **15**, 145 (1993).
- [11] J. Carlson, Phys. Rev. C**36**, 2026 (1987), Phys. Rev. C**38**, 1879 (1988); J.G. Zabolitzki, K.E. Schmidt, and M.H. Kalos, Phys. Rev. C**25**, 1111 (1982); J. Carlson and R. Schiavilla, Rev. Mod. Phys. **70**, 743 (1998).
- [12] Ch. Elster, W. Schadow, A. Nogga, and W. Glöckle, Few-Body System, **27**, 83 (1998).
- [13] W. Schadow, Ch. Elster, and W. Glöckle, Few-Body Systems **28**, 15 (2000).
- [14] A.A. Kvitsinsky and C.-Y. Hu, Few-Body Systems **12**, 7 (1992).
- [15] I. Fachruddin, Ch. Elster, W. Glöckle, Phys. Rev. C**62**, 044002-1 (2000).
- [16] W. Glöckle, The Quantum Mechanical Few-Body Problem, Springer-Verlag (1983).
- [17] S.A. Coon and W. Glöckle, Phys. Rev. C**23**, 1790 (1981).
- [18] D. Hüber, H. Witala, A. Nogga, W. Glöckle and H. Kamada, Few-Body System, **22**, 107 (1997).
- [19] J. Fujita, H. Miyazawa, Prog. Theor. Phys. **17**, 360 (1957).
- [20] Ch. Elster, E.E. Evans, H. Kamada and W. Glöckle, Few-Body System, **21**, 25 (1996).
- [21] Ch. Elster, J.H. Thomas, W. Glöckle, Few-Body Systems, **24**, 55 (1998).
- [22] A. Nogga, PhD Thesis, Ruhr-University Bochum, 2001.
- [23] A. Nogga, D. Hüber, H. Kamada, W. Glöckle, Phys. Lett. B**409**, 19 (1997).
- [24] A. Saake, Diploma Thesis, Ruhr-University Bochum, 1992 (unpublished).
- [25] W. Glöckle, T.-S.H. Lee, F. Coester, Phys. Rev. C**33**, 709 (1986).
- [26] H. Kamada, Few-Body Systems, Suppl. **12**, 433 (2000).

TABLES

TABLE I. The parameters of the MT2-II two-body force.

$g_A^2/4\pi$	m_A [MeV]	Λ_A [MeV]	$g_R^2/4\pi$	m_R [MeV]	Λ_R [MeV]
3.5775	330.2104	1500.0	9.4086	612.4801	1500.0

TABLE II. The parameters of the MT3-I attractive 3BF.

$g_\alpha^2/4\pi$	m_α [MeV]	Λ_α [MeV]	a_α
5.0	305.8593	1000.0	-1.73

TABLE III. The calculated eigenvalue E from the the solution of the Faddeev equation and the expectation values of the kinetic energy $\langle H_0 \rangle$, the two-body potential $\langle V_{II} \rangle$, the three-body potential energy $\langle V_{123} \rangle$ and the total Hamiltonian $\langle H \rangle$ as functions of the number of grid points NP, NQ and NX for the $p - q - x$ grid. The calculations are based on the MT2-II 2BF and the MT3-I 3BF.

NP	NQ	NX	$\langle H_0 \rangle$ (MeV)	$\langle V_{II} \rangle$ (MeV)	$\langle V_{123} \rangle$ (MeV)	$\langle H \rangle$ (MeV)	E (MeV)
45	45	42	31.8838	-39.4069	-1.3392	-8.8623	-8.8715
61	45	42	31.8846	-39.4073	-1.3396	-8.8623	-8.8711
77	45	42	31.8848	-39.4074	-1.3397	-8.8623	-8.8709
77	61	42	31.8900	-39.4133	-1.3406	-8.8639	-8.8726
77	77	42	31.8915	-39.4149	-1.3409	-8.8643	-8.8731
87	87	42	31.8919	-39.4152	-1.3410	-8.8644	-8.8732
97	97	42	31.8920	-39.4154	-1.3410	-8.8644	-8.8732

TABLE IV. The calculated eigenvalue E of the Faddeev equation and the expectation values of the kinetic energy $\langle H_0 \rangle$, the two-body potential $\langle V_{II} \rangle$, and the total Hamiltonian $\langle H \rangle$ as functions of the number of grid points NP, NQ and NX for the $p - q - x$ grid. The calculations are based on the MT2-II 2BF alone.

NP	NQ	NX	$\langle H_0 \rangle$ (MeV)	$\langle V_{II} \rangle$ (MeV)	$\langle H \rangle$ (MeV)	E (MeV)
77	77	42	28.6408	-36.3390	-7.6983	-7.6984
87	87	42	28.6408	-36.3391	-7.6983	-7.6984
97	97	42	28.6408	-36.3392	-7.6983	-7.6984

TABLE V. The parameters of the MT3-II 3BF.

$g_\alpha^2/4\pi$	m_α [MeV]	Λ_α [MeV]	a_α
5.0	305.8593	1000.0	-2.69
$g_\rho^2/4\pi$	m_ρ [MeV]	Λ_ρ [MeV]	$a_{\alpha\rho}$
9.0	650.0000	1900.0	2.40

TABLE VI. The calculated eigenvalue E from the the solution of the Faddeev equation and the expectation values of the kinetic energy $\langle H_0 \rangle$, the two-body potential $\langle V_{II} \rangle$, the three-body potential energy $\langle V_{123} \rangle$ and the total Hamiltonian $\langle H \rangle$ as functions of the number of grid points NP, NQ and NX for the $p - q - x$ grid. The calculations are based on the MT2-II 2BF and the MT3-II 3BF.

NP	NQ	NX	$\langle H_0 \rangle$ (MeV)	$\langle V_{II} \rangle$ (MeV)	$\langle V_{123} \rangle$ (MeV)	$\langle H \rangle$ (MeV)	E (MeV)
45	45	42	31.1745	-38.7859	-1.0404	-8.6518	-8.6454
61	45	42	31.1767	-38.7878	-1.0409	-8.6520	-8.6456
77	45	42	31.1773	-38.7881	-1.0413	-8.6521	-8.6466
77	61	42	31.1825	-38.7880	-1.0478	-8.6533	-8.6477
77	77	42	31.1837	-38.7886	-1.0481	-8.6530	-8.6480
87	87	42	31.1842	-38.7887	-1.0481	-8.6526	-8.6478
97	97	42	31.1847	-38.7892	-1.0481	-8.6526	-8.6478

TABLE VII. The expectation values of the kinetic energy $\langle H_0 \rangle$, the two-body potential MT2-II, $\langle V_{II} \rangle$, the three-body potential $\langle V_{123} \rangle$, and the total Hamiltonian $\langle H \rangle$ calculated with different strengths of the 3BF MT3-I.

	$\langle H_0 \rangle$ (MeV)	$\langle V_{II} \rangle$ (MeV)	$\langle V_{123} \rangle$ (MeV)	$\langle H \rangle$ (MeV)
a_α	31.8919	-39.4153	-1.3410	-8.8644
$2a_\alpha$	36.1500	-42.9119	-3.6316	-10.3934
$4a_\alpha$	50.2537	-50.4037	-15.2166	-15.3666
$6a_\alpha$	82.7022	-49.8850	-59.0747	-26.2575
$8a_\alpha$	158.357	-0.4563	-219.381	-61.4800

TABLE VIII. The expectation values of the kinetic energy $\langle H_0 \rangle$, the two-body potential $\langle V_{II} \rangle$, the three-body potential $\langle V_{123} \rangle$, and the total Hamiltonian $\langle H \rangle$ energies calculated with different strengths of the MT3-II 3BF.

	$\langle H_0 \rangle$ (MeV)	$\langle V_{II} \rangle$ (MeV)	$\langle V_{123} \rangle$ (MeV)	$\langle H \rangle$ (MeV)
$a_\alpha, a_{\alpha\rho}$	31.6662	-39.2386	-1.2581	-8.8305
$2a_\alpha, 2a_{\alpha\rho}$	34.1243	-41.4718	-2.4629	-9.8104
$4a_\alpha, 4a_{\alpha\rho}$	41.0706	-47.0688	-6.6948	-12.6929
$8a_\alpha, 8a_{\alpha\rho}$	59.5265	-58.1352	-23.0029	-21.6117
$16a_\alpha, 16a_{\alpha\rho}$	107.559	-71.5472	-91.8266	-55.8151

TABLE IX. The binding energy E , and the expectation values $\langle r \rangle$ and $\langle R \rangle$ calculated with different coupling constants a_α of the purely attractive 3BF MT3-I. All calculations are based on the MT2-II 2BF and MT3-I 3BF. The deviation δ characterizes the deviation from the shape of an equilateral triangle and is defined in Eq. (4.15).

	a_α	$2a_\alpha$	$3a_\alpha$	$4a_\alpha$
E (MeV)	-8.873	-10.447	-12.640	-15.936
$\langle r \rangle$ (fm)	2.382	2.230	2.063	1.878
$\langle R \rangle$ (fm)	2.096	1.960	1.813	1.650
δ (%)	1.61	1.49	1.48	1.45

TABLE X. The binding energy E , and the expectation values $\langle r \rangle$ and $\langle R \rangle$ calculated with different exchange masses m_α of the purely attractive 3BF MT3-I. All calculations are based on the MT2-II 2BF and MT3-I 3BF. The deviation δ characterizes the deviation from the shape of an equilateral triangle and is defined in Eq. (4.15).

	m_α	$m_\alpha - 50$	$m_\alpha - 100$	$m_\alpha - 150$
E (MeV)	-8.873	-10.238	-13.182	-20.796
$\langle r \rangle$ (fm)	2.382	2.255	2.058	1.771
$\langle R \rangle$ (fm)	2.096	1.983	1.809	1.558
δ (%)	1.61	1.54	1.50	1.59

TABLE XI. The parameters of the attractive MT2-I 2BF.

$g_A^2/4\pi$	m_A [MeV]	Λ_A [MeV]
-0.7210	330.2104	1500.0

TABLE XII. The parameters of the purely attractive MMT3-I 3BF.

$g_\alpha^2/4\pi$	m_α [MeV]	Λ_α [MeV]	a_α
5.0000	305.8593	1000.0	-9.34

TABLE XIII. The parameters of the MMT3-II 3BF.

$g_\alpha^2/4\pi$	m_α [MeV]	Λ_α [MeV]	a_α
5.0000	305.8593	1000.0	-26.96
$g_\rho^2/4\pi$	m_ρ [MeV]	Λ_ρ [MeV]	$a_{\alpha\rho}$
9.0000	650.0000	1900.0	15.98

TABLE XIV. The expectation values of the kinetic energy $\langle H_0 \rangle$, the two-body potential $\langle V_{II} \rangle$, the three-body potential $\langle V_{123} \rangle$, the binding energy E , and the shape parameters $\langle r \rangle$ and $\langle R \rangle$ for the models MT2-I, MT2-II, MMT3-I and MMT3-II.

	MT2-I	MT2-II	MMT3-I	MMT3-II
$\langle H_0 \rangle$ (MeV)	66.967	28.641	280.657	135.332
$\langle V_{II} \rangle$ (MeV)	-74.547	-36.339	—	—
$\langle V_{123} \rangle$ (MeV)	—	—	-288.210	-142.914
E (MeV)	-7.5803	-7.6980	-7.5535	-7.5815
$\langle r \rangle$ (fm)	1.783	2.521	0.864	1.170
$\langle R \rangle$ (fm)	1.592	2.221	0.783	1.019

FIGURES

FIG. 1. Diagrammatic representation of the three-body force $V_4^{(1)}$. Here particle (1) is singled out by the meson-nucleon amplitude described by the blob. The three-body force is then given according to Eq. (2.2).

FIG. 2. The momentum distributions $n(q)$ calculated with the MT2-II two-body potential and the MT3-I three-body potential (solid line). The other lines represent calculations in which the strength parameters a_α of the 3BF MT3-I is increased by even integers as indicated in the legend.

FIG. 3. Same as Fig. 2, except that the exchange mass m_α of the MT3-I three-body potential is decreased.

FIG. 4. The momentum distributions $n(q)$ calculated with the MT2-II two-body potential and the MT3-II three-body potential (solid line). The other lines represent calculations in which the strength parameters a_α and $a_{\alpha\rho}$ of the 3BF MT3-II are increased by even integers as indicated in the legend.

FIG. 5. The two-body correlation function $c(r)$ calculated with the MT2-II two-body potential and the MT3-I three-body potential (solid line). The other lines represent calculations in which the strength parameters a_α of the 3BF MT3-I is increased by even integers as indicated in the legend.

FIG. 6. Same as Fig. 5, except that the exchange mass m_α of the MT3-I three-body potential is decreased.

FIG. 7. The two-body correlation function $c(r)$ calculated with the MT2-II two-body potential and the MT3-II three-body potential (solid line). The other lines represent calculations in which the strength parameters a_α and $a_{\alpha\rho}$ of the 3BF MT3-II are increased by even integers as indicated in the legend.

FIG. 8. The momentum distribution $n(q)$ calculated with the different models described in Section V.

FIG. 9. The two-body correlation function $c(r)$ calculated with the different models described in Section V.

FIG. 10. The magnitude of the 3N bound state wave function $\Psi(p, q, x)$ for $x = 1$ in units of fm^3 calculated with the model MT2-I, consisting of a purely attractive 2BF with parameters given in Table XI.

FIG. 11. The magnitude of the 3N bound state wave function $\Psi(p, q, x)$ for $x = 1$ in units of fm^3 calculated with the model MT2-II, consisting of a 2BF with short-range repulsion and intermediate-range attraction with parameters given in Table I.

FIG. 12. The magnitude of the 3N bound state wave function $\Psi(p, q, x)$ for $x = 1$ in units of fm^3 calculated with the model MMT3-I, consisting of a purely attractive 3BF with parameters given in Table XII.

FIG. 13. The magnitude of the 3N bound state wave function $\Psi(p, q, x)$ for $x = 1$ in units of fm^3 calculated with the model MMT3-II, consisting of a 3BF with short-range repulsion and intermediate-range attraction with parameters given in Table XIII.

FIG. 14. The momentum distributions $n(q)$ calculated with the attractive 2BF MT2-I (solid line). The two dashed curves represent calculations with two different purely attractive 3BFs, (A) and (B), where the parameters are chosen such that the binding energy and the momentum distribution are similar to the one given by the MT2-I potential.

FIG. 15. The two-body correlation function $c(r)$ calculated with the attractive 2BF MT2-I (solid line). The two dashed curves represent calculations with the two different purely attractive 3BFs, (A) and (B), as shown in Fig. 14 and described in Section V.

Fig.1

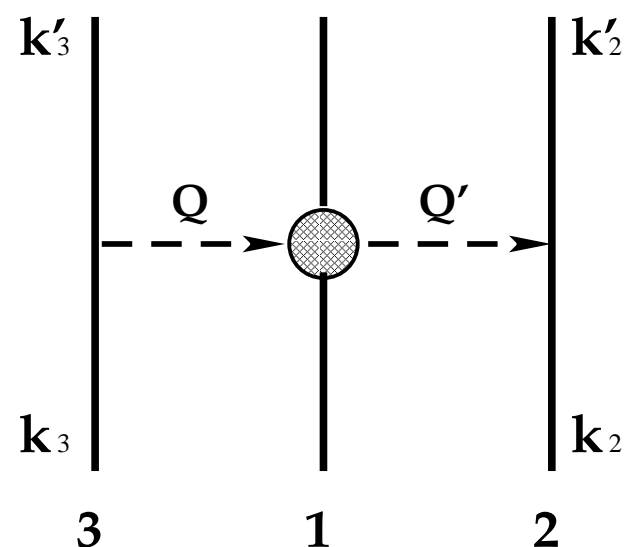


Fig.2

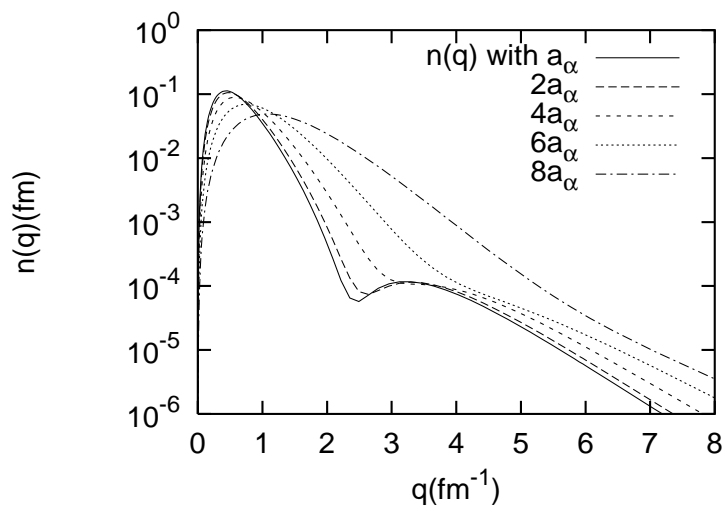


Fig.3

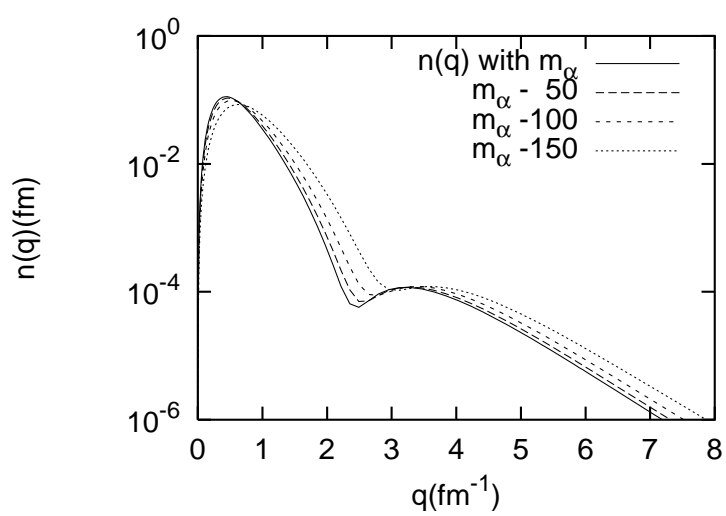


Fig.4

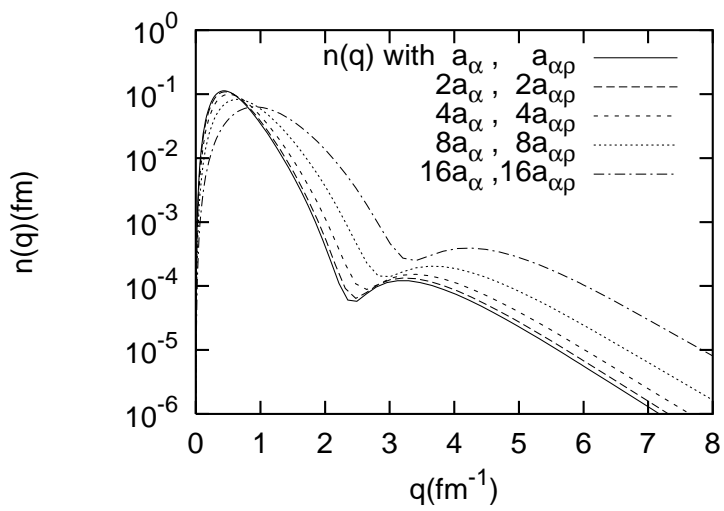


Fig.5

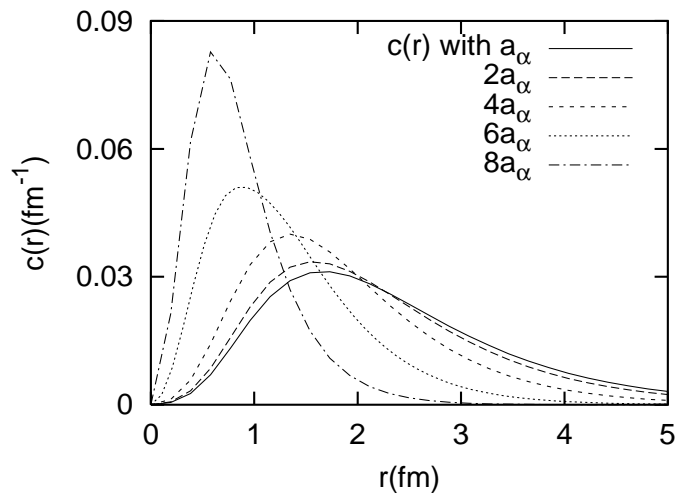


Fig.6

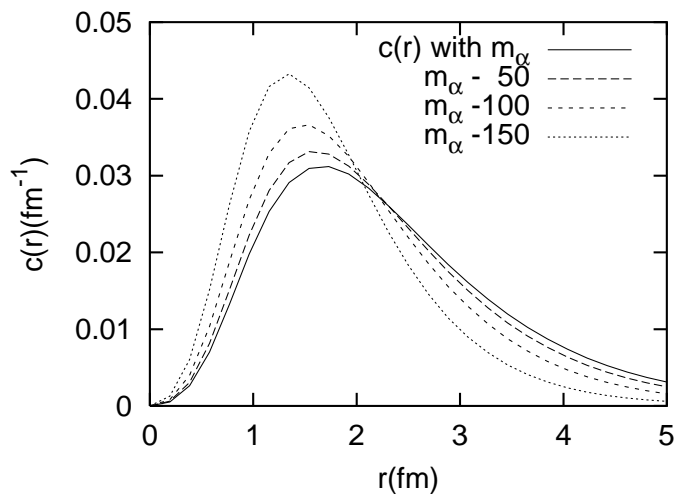


Fig.7

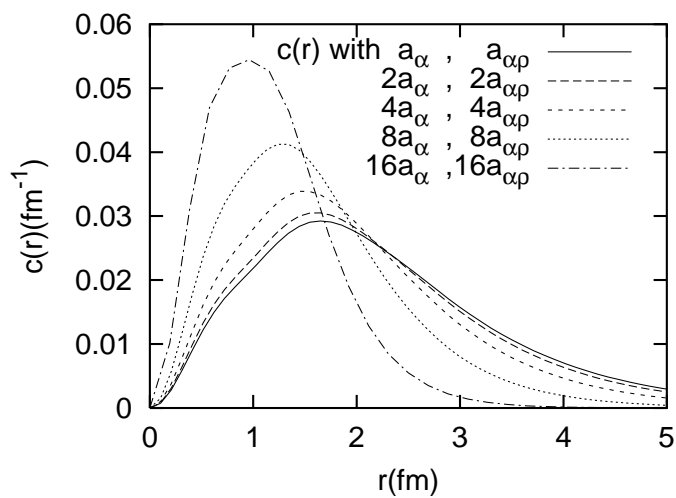


Fig.8

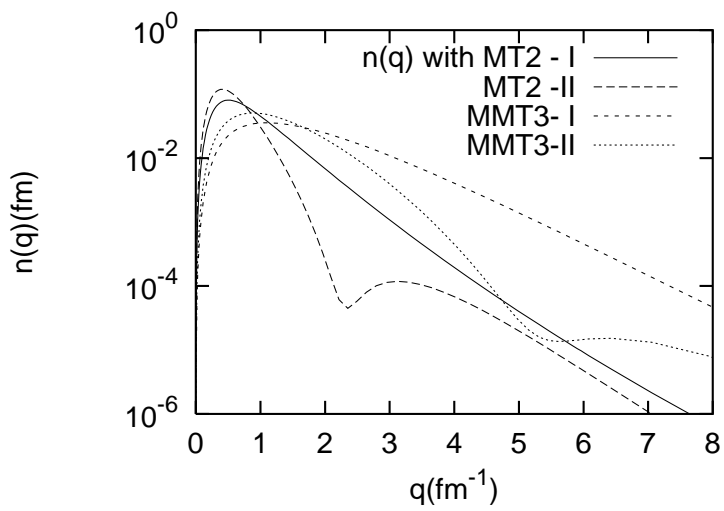


Fig.9

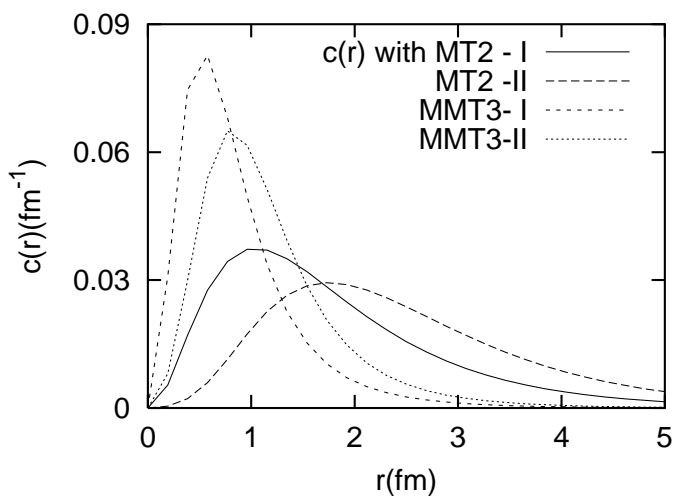


Fig.10

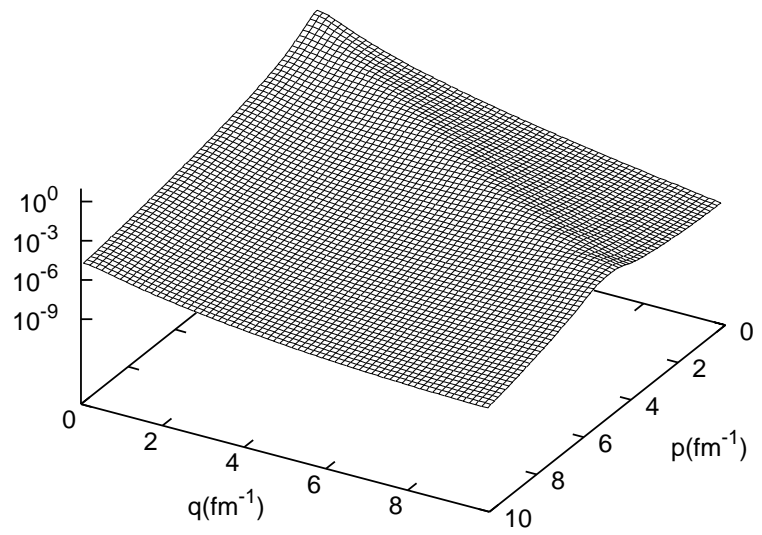


Fig.11

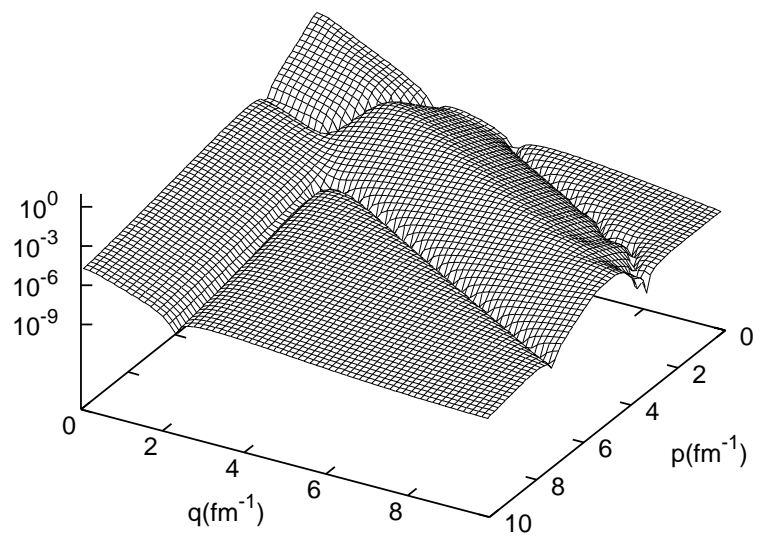


Fig.12

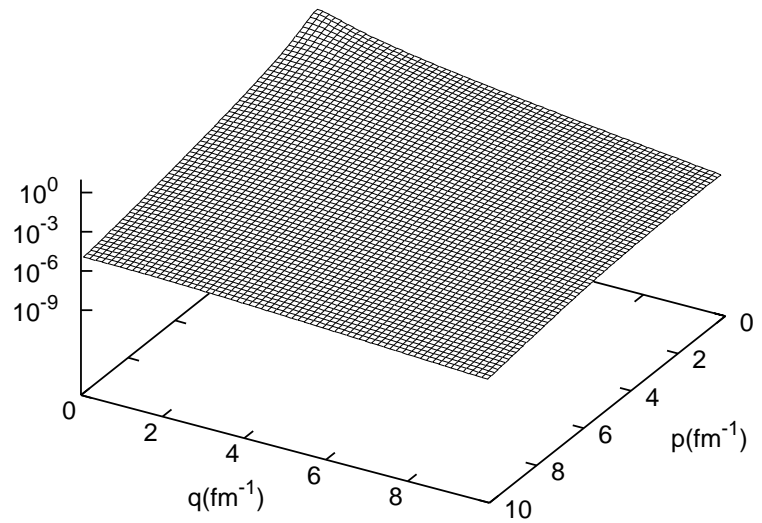


Fig.13

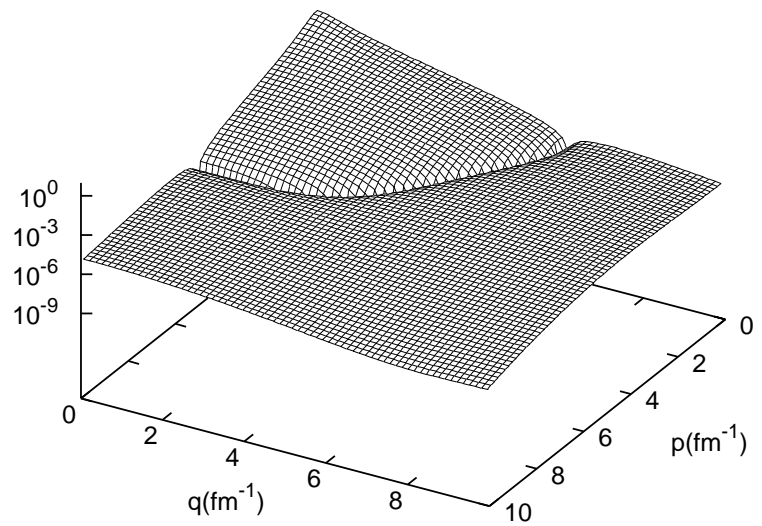


Fig.14

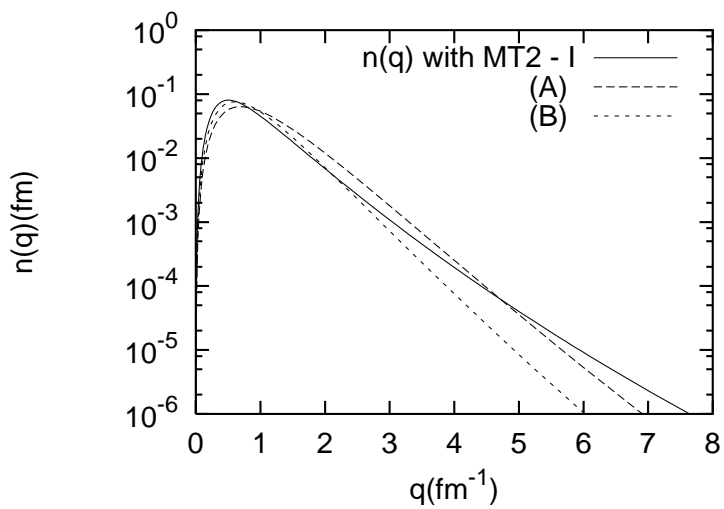


Fig.15

